

Second-order charge and spin transport in LaO/STO system in the presence of cubic Rashba spin orbit couplings

Zhuo Bin Siu,^{1,*} Anirban Kundu,^{1,2,†} and Mansoor B.A. Jalil^{1,‡}

¹*Department of Electrical and Computer Engineering,
National University of Singapore, Singapore 117583, Republic of Singapore*
²*Department of Physics, Ariel University, Ariel 40700, Israel*

Certain non-centrosymmetric materials with broken time-reversal symmetry may exhibit non-reciprocal transport behavior under an applied electric field in which the charge and spin currents contain components that are second order in the electric field. In this study, we investigate the second-order spin accumulation and charge and spin responses in the LaAlO₃/SrTiO₃ (LaO/STO) system with magnetic dopants under the influence of linear and cubic Rashba spin-orbit coupling (RSOC) terms. We explain the physical origin of the second-order response and perform a symmetry analysis of the first and second-order responses for different dopant magnetization directions relative to the applied electric field. We then numerically solve the Boltzmann transport equation by extending the approach of Schliemann and Loss [Phys. Rev. B 68, 165311] to higher orders in the electric field. We show that the sign of the second-order responses can be switched by varying the magnetization direction of the magnetic dopants or relative strengths of the two cubic RSOC terms and explain these trends by considering the Fermi surfaces of the respective systems. These findings provide insights into the interplay of multiple SOC effects in a LaO/STO system and how the resulting first- and second-order charge and spin responses can be engineered by exploiting the symmetries of the system.

I. INTRODUCTION

A characteristic of non-centrosymmetric materials with broken time-reversal symmetry is non-reciprocal transport behavior in which charge currents flowing along opposite directions experience different electrical resistivities. Such non-reciprocal transport has been experimentally observed in, e.g., the bulk polar semiconductor BiTeBr [1] and the transition metal dichalcogenide WTe₂ [2] and can be interpreted as an electrical resistance that is itself linearly dependent on the applied electric field, thus giving rise to a quadratic dependence of the current on the electric field. This second-order response can be exploited to characterize the surface spin texture [3, 4] or the strength of the Rashba spin-orbit interaction in a material [1]. Such second-order responses can be generalized to other transport quantities aside from the longitudinal current. For instance, a second-order Hall current perpendicular to the electric field has been observed in WTe₂ [5]. Additionally, a second-order response in the spin current has also been demonstrated in the presence of an applied AC field, which when coupled with the absence of a corresponding first-order response in the charge current results in the generation of pure spin current without an accompanying charge current [6, 7],

In particular, large second-order responses for the charge current have been experimentally observed in the LaAlO₃/SrTiO₃ (LaO/STO) system [8–10]. The LaO/STO system is a promising candidate material for spintronics applications because of the strong spin-orbit coupling at its interface, which gives rise to a large (first-order) spin-to-charge conversion efficiency [11–13]. Besides the usual $\alpha(\mathbf{k} \times \boldsymbol{\sigma}) \cdot \hat{z}$ linear Rashba spin-orbit coupling (SOC) term, there is also a significant cubic-momentum Rashba SOC at the LaO/STO interface [14–16]. In the LaO/STO system, the linear RSOC has a strength of approximately 10 meVÅ and that of the cubic RSOC is approximately 1–5 eVÅ³ [15, 17–19]. When considered over the Brillouin zone, the linear and cubic SOC energy splits in the LaO/STO system are comparable in magnitude.

Recently, Ho et al. showed that the low-energy Hamiltonian for the LaO/STO system can be described as comprising the usual linear Rashba SOC and two distinct types of cubic Rashba SOC terms. The magnitudes of the three SOC terms can be externally tuned by modulating the thickness of the two-dimensional electron gas at the LaO/STO interface and the out-of-plane electric field [19]. In general, the cubic SOC terms play a key role in inducing non-linear spin and current responses. For example, it has been predicted that the trigonal warping term in transition metal dichalcogenides can give rise to non-linear spin current [6], whereas in Bi₂Te₃, which is a topological insulator, the experimentally observed nonlinear magnetoresistance [3] and Hall current [7] were attributed to the hexagonal warping [20–22] of its Fermi surface due to the cubic SOC terms. However, to the best of our knowledge, the effects

* elesiuz@nus.edu.sg

† anirbank5@gmail.com

‡ elembaj@nus.edu.sg

of these cubic Rashba terms on the second-order transport phenomena such as the transverse charge current and spin accumulation have not yet been studied.

Therefore, in this study, we investigate the second-order charge current, spin accumulation, and spin current in the LaO/STO system in the presence of the linear and the two distinct cubic Rashba SOC terms. We apply the Boltzmann transport model and solve it to the second order in the applied electric field. We adopt the more refined scattering model of Schliemann and Loss [23] (SL), which yields a more accurate representation up to the higher orders compared to the relaxation time approximation (RTA). The SL approach is first extended to higher orders in the applied electric field and then used to solve the Boltzmann model. We elucidate the physical origin of the second-order charge and spin transport responses by considering the symmetry of the first- and second-order responses. Based on the symmetry analysis, we explain how the second-order responses vary as functions of the strengths of the various SOC terms as well as the magnetization coupling.

II. EXTENSION OF SCHLIEMANN-LOSS APPROACH

The Boltzmann equation for a time-invariant homogeneous system with an applied electric field \mathbf{E} is given by

$$e\mathbf{E} \cdot \partial_{\mathbf{k}} f_{\mu}(\mathbf{k}) = \partial_t f_{\mu}(\mathbf{k}), \quad (1)$$

where $f_{\mu}(\mathbf{k})$ is the occupation function of the μ th band.

We assume that $\partial_t f_{\mu}(\mathbf{k})$ has the general form of

$$\partial_t f_{\mu}(\mathbf{k}) = -S[f_{\mu}(\mathbf{k})] \quad (2)$$

where $S[f_{\mu}]$ denotes that S is a functional of f_{μ} . In the commonly adopted RTA approach, $S[f_{\mu}]$ is assumed to have the form of $S[f_{\mu}] = (f_{\mu} - f^{(0)})/\tau$ where τ is a constant relaxation time and $f^{(0)}$ is the Fermi–Dirac distribution. Subsequently, a more refined approximation for the scattering functional was adopted by Schliemann and Loss who assumed a collision integral in the form of [24]

$$S[f_{\mathbf{k}}] = \int d\mathbf{k}' \sum_{\mu, \mu'} w_{\mathbf{k}, \mu, \mathbf{k}', \mu'} (f_{\mu}(\mathbf{k}) - f_{\mu'}(\mathbf{k}')) \quad (3)$$

where $w_{\mathbf{k}, \mu, \mathbf{k}', \mu'}$ is the transition probability for electrons in the (\mathbf{k}, μ) state to be scattered into the (\mathbf{k}', μ') state. We consider electrons to be scattered by impurities, each of which is modeled as a delta function potential

$$V_i(\mathbf{r}) = a_0 V_0 \delta(\mathbf{r} - \mathbf{R}_i) \quad (4)$$

where \mathbf{R}_i is the spatial location of the impurity, V_0 its scattering strength, and a_0 is a quantity with the physical dimensions of area introduced for dimensional consistency [25]. Denoting the number density (i.e., the number per unit area) of such impurities as n and applying the Fermi golden rule, the transition rate due to all the impurities is given by

$$w_{\mathbf{k}, \mu, \mathbf{k}', \mu'} = 2\pi n |\langle \mathbf{k}, \mu | a_0 V_0 | \mathbf{k}', \mu' \rangle|^2 \delta(\epsilon_{\mu}(\mathbf{k}) - \epsilon_{\mu'}(\mathbf{k}')). \quad (5)$$

In analogy to the Schliemann and Loss approach [23], let $\theta_{\mu}(\mathbf{k})$ be the angle between the direction of the velocity $\langle \mathbf{v} \rangle$ for the state at \mathbf{k} on the μ th band and the applied electric field \mathbf{E} . Consider

$$\begin{aligned} & S[v_{\mu}(\mathbf{k}) \exp(i\theta_{\mu}(\mathbf{k}))] \\ &= \sum_{\mu'} \int \frac{dS_{\mathbf{k}'}}{2\pi^2} (v_{\mu}(\mathbf{k}) \exp(i\theta_{\mu}(\mathbf{k})) - v_{\mu'}(\mathbf{k}') \exp(i\theta_{\mu'}(\mathbf{k}'))) w_{\mathbf{k}, \mu, \mathbf{k}', \mu'} \end{aligned} \quad (6)$$

$$= \left[\sum_{\mu'} \int \frac{dS_{\mathbf{k}'}}{2\pi^2} \left(1 - \frac{v_{\mu'}(\mathbf{k}')}{v_{\mu}(\mathbf{k})} \exp(i(\theta_{\mu'}(\mathbf{k}') - \theta_{\mu}(\mathbf{k}))) \right) w_{\mathbf{k}, \mu, \mathbf{k}', \mu'} \right] v_{\mu}(\mathbf{k}) \exp(i\theta_{\mu}(\mathbf{k})). \quad (7)$$

By comparing the real and imaginary parts, we have

$$\begin{aligned}
& S[v_\mu(\mathbf{k}) \cos(\theta_\mu(\mathbf{k}))] \\
&= \sum_{\mu'} \int \frac{dS_k}{(2\pi)^2} \left[- \left(\frac{v_{\mu'}(\mathbf{k}')}{v_\mu(\mathbf{k})} \sin(\theta_{\mu'}(\mathbf{k}') - \theta_\mu(\mathbf{k})) \right) v_\mu(\mathbf{k}) \sin(\theta_\mu(\mathbf{k})) \right. \\
&\quad \left. + \left(1 - \frac{v_{\mu'}(\mathbf{k}')}{v_\mu(\mathbf{k})} \cos(\theta_{\mu'}(\mathbf{k}') - \theta_\mu(\mathbf{k})) \right) v_\mu(\mathbf{k}) \cos(\theta_\mu(\mathbf{k})) \right] w_{\mathbf{k},\mu,\mathbf{k}',\mu'}, \tag{8}
\end{aligned}$$

$$\begin{aligned}
& S[v_\mu(\mathbf{k}) \sin(\theta_\mu(\mathbf{k}))] \\
&= \sum_{\mu'} \int \frac{dS_k}{(2\pi)^2} \left[- \left(\frac{v_{\mu'}(\mathbf{k}')}{v_\mu(\mathbf{k})} \sin(\theta_{\mu'}(\mathbf{k}') - \theta_\mu(\mathbf{k})) \right) v_\mu(\mathbf{k}) \cos(\theta_\mu(\mathbf{k})) \right. \\
&\quad \left. + \left(1 - \frac{v_{\mu'}(\mathbf{k}')}{v_\mu(\mathbf{k})} \cos(\theta_{\mu'}(\mathbf{k}') - \theta_\mu(\mathbf{k})) \right) v_\mu(\mathbf{k}) \sin(\theta_\mu(\mathbf{k})) \right] w_{\mathbf{k},\mu,\mathbf{k}',\mu'}. \tag{9}
\end{aligned}$$

We define

$$(\tau_\mu^\parallel(\mathbf{k}))^{-1} = \sum_{\mu'} \int \frac{dS_k}{(2\pi)^2} w_{\mathbf{k},\mu,\mathbf{k}',\mu'} \left(1 - \frac{v_{\mu'}(\mathbf{k}')}{v_\mu(\mathbf{k})} \cos(\theta_{\mu'}(\mathbf{k}') - \theta_\mu(\mathbf{k})) \right) \tag{10}$$

$$(\tau_\mu^\perp(\mathbf{k}))^{-1} = \sum_{\mu'} \int \frac{dS_k}{(2\pi)^2} w_{\mathbf{k},\mu,\mathbf{k}',\mu'} \left(\frac{v_{\mu'}(\mathbf{k}')}{v_\mu(\mathbf{k})} \sin(\theta_\mu(\mathbf{k}) - \theta_{\mu'}(\mathbf{k}')) \right), \tag{11}$$

so that the scattering functionals can be written as

$$S \begin{bmatrix} v_\mu(\mathbf{k}) \cos(\theta_\mu(\mathbf{k})) \\ v_\mu(\mathbf{k}) \sin(\theta_\mu(\mathbf{k})) \end{bmatrix} = \begin{pmatrix} (\tau_\mu^\parallel(\mathbf{k}))^{-1} & -\tau_\mu^\perp(\mathbf{k})^{-1} \\ \tau_\mu^\perp(\mathbf{k})^{-1} & \tau_\mu^\parallel(\mathbf{k})^{-1} \end{pmatrix} \begin{pmatrix} v_\mu(\mathbf{k}) \cos(\theta_\mu(\mathbf{k})) \\ v_\mu(\mathbf{k}) \sin(\theta_\mu(\mathbf{k})) \end{pmatrix}. \tag{12}$$

To extend the SL formalism to higher orders in \mathbf{E} , we expand $f_\mu(\mathbf{k})$ as a series in $E = |\mathbf{E}|$, i.e., $f_\mu(\mathbf{k}) = \sum_n f_\mu^{(n)}(\mathbf{k}) E^n$.

To the first order in E , Eq. (1) gives

$$(e\mathbf{E} \cdot \partial_{\mathbf{k}} \epsilon) \partial_\epsilon f^{(0)}(\mathbf{k}) = -S[f_\mu^{(1)}(\mathbf{k})E]. \tag{13}$$

We apply the ansatz

$$f_\mu^{(1)}(\mathbf{k})E = eE(\partial_\epsilon f^{(0)}(\mathbf{k}))(c^{(1)}v_\mu(\mathbf{k}) \cos(\theta_\mu(\mathbf{k})) + s^{(1)}v_\mu(\mathbf{k}) \sin(\theta_\mu(\mathbf{k}))) \tag{14}$$

where $c^{(1)}$ and $s^{(1)}$ are unknown coefficients to be determined. Based on Eq. (12), Eq. (13) reduces to (we drop the \mathbf{k} arguments here for notational simplicity)

$$-\cos(\theta_\mu) = c^{(1)} \left((\tau_\mu^\parallel)^{-1} \cos(\theta_\mu) - (\tau_\mu^\perp)^{-1} \sin(\theta_\mu) \right) + s^{(1)} \left((\tau_\mu^\perp)^{-1} \cos(\theta_\mu) + (\tau_\mu^\parallel)^{-1} \sin(\theta_\mu) \right). \tag{15}$$

Comparing the coefficients of $\cos(\theta_\mu)$ and $\sin(\theta_\mu)$ on both sides of the equation, we have

$$\left(c^{(1)}(\tau_\mu^\parallel)^{-1} + s^{(1)}(\tau_\mu^\perp)^{-1} \right) = -1, \tag{16}$$

$$\left(c^{(1)}(-\tau_\mu^\perp)^{-1} + s^{(1)}(\tau_\mu^\parallel)^{-1} \right) = 0. \tag{17}$$

This gives

$$c^{(1)} = -\frac{\tau_\mu^\parallel}{1 + \left(\frac{\tau_\mu^\parallel}{\tau_\mu^\perp} \right)^2} \tag{18}$$

$$s^{(1)} = -\frac{\tau_\mu^\perp}{1 + \left(\frac{\tau_\mu^\perp}{\tau_\mu^\parallel} \right)^2}. \tag{19}$$

The second-order terms in \mathbf{E} in Eq. (1) read

$$e\mathbf{E} \cdot \partial_{\mathbf{k}} f_{\mu}^{(1)} E_{\mu} = -S[f_{\mu}^{(2)} E^2], \quad (20)$$

$$\Rightarrow ev_{\mu} \cos(\theta_{\mu})(\partial_{\epsilon} f_{\mu}^{(1)}) = -S[f_{\mu}^{(2)}]. \quad (21)$$

In analogy to Eqs. (13) and (14), this suggests that we can adopt a similar ansatz in Eq. (21):

$$f_{\mu}^{(2)} = e(\partial_{\epsilon} f_{\mu}^{(1)})(c^{(2)}v_{\mu}(\mathbf{k}) \cos(\theta_{\mu}(\mathbf{k})) + s^{(2)}v_{\mu}(\mathbf{k}) \sin(\theta_{\mu}(\mathbf{k}))) \quad (22)$$

This gives an analogous set of equations to Eq. (17) with the $c^{(1)}$ and $s^{(1)}$ replaced by $c^{(2)}$ and $s^{(2)}$, respectively. $c^{(2)}$ and $s^{(2)}$ therefore have the same forms as $c^{(1)}$ and $s^{(1)}$, respectively.

Generalizing the above results, we see that the n th order term in the expansion of the occupation function is given by

$$E f_{\mu}^{(n)}(\mathbf{k}) = - \left[eE v_{\mu}(\mathbf{k}) \left(\frac{\tau_{\mu}^{\parallel}(\mathbf{k})}{1 + \left(\frac{\tau_{\mu}^{\parallel}(\mathbf{k})}{\tau_{\mu}^{\perp}(\mathbf{k})}\right)^2} \cos(\theta_{\mu}(\mathbf{k})) + \frac{\tau_{\mu}^{\perp}(\mathbf{k})}{1 + \left(\frac{\tau_{\mu}^{\perp}(\mathbf{k})}{\tau_{\mu}^{\parallel}(\mathbf{k})}\right)^2} \sin(\theta_{\mu}(\mathbf{k})) \right) \right] (\partial_{\epsilon} f_{\mu}^{(n-1)}(\mathbf{k})). \quad (23)$$

In contrast to the conventional RTA in which a constant \mathbf{k} -independent relaxation time τ is used for all states on all bands, the scattering in the SL approach now differs for each state. Moreover, the SL approach allows for the possibility that change in momentum may be perpendicular to the direction of the electric field as denoted by the $\sin(\theta_{\mu}(\mathbf{k}))$ terms, unlike the RTA in which the change in momentum is restricted to being parallel to the applied electric field.

A. Physical interpretation of first- and second-order terms

Because the terms in the large round brackets in Eq. (23) have the dimensions of time, their product with eE have the dimensions of \mathbf{k} . This product can thus be interpreted as the \mathbf{k} -space shift of the Fermi surface induced by the electric field. The terms in the square brackets in Eq. (23) in turn have the dimensions of energy and can be interpreted as the energy shift induced by the shift in the Fermi surface. Denoting these terms as $\delta\epsilon_{\mu}$ and introducing $\delta f_{\mu}^{(n)} \equiv E^n f_{\mu}^{(n)}$, we have, explicitly,

$$\delta f_{\mu}^{(1)} = -(\delta\epsilon_{\mu})(\partial_{\epsilon} f_{\mu}^{(0)}), \quad (24)$$

$$\delta f_{\mu}^{(2)} = -(\delta\epsilon_{\mu})(\partial_{\epsilon} \delta f_{\mu}^{(1)}). \quad (25)$$

We note that Eqs. (24) and (25) are also applicable to the conventional RTA approach, for which $\delta\epsilon_{\mu} = v_{\mu} \cos(\theta_{\mu}) E \tau$ where τ is the RTA relaxation time. In this section and the next sections, we base our explanation on the RTA for expositional simplicity although the arguments can be readily extended to the SL approach by using the appropriate $\delta\epsilon_{\mu}$ given in Eq. (23). Figure S1 in the Supplemental Materials show that the RTA and SL approaches produce qualitatively similar results except for a small underestimation of the magnitudes of the second-order responses by the RTA approach.

The first-order response $\delta O^{(1)}$ of an observable quantity O (e.g., the x and y velocities $v_{x,y}$ or spin polarizations $\sigma_{x,y}$) to the electric field is given by

$$\delta O^{(1)} = \int d\mathbf{k} \left(\sum_{\mu} \delta f_{\mu}^{(1)}(\mathbf{k}) O_{\mu}(\mathbf{k}) \right) \quad (26)$$

where $O_{\mu}(\mathbf{k}) \equiv \langle \mathbf{k}; \mu | O | \mathbf{k}; \mu \rangle$ is the expectation value of the quantity. Substituting Eq. (24) into Eq. (26), the $\delta f_{\mu}^{(1)}(\mathbf{k}) O_{\mu}(\mathbf{k})$ term becomes $(-\partial_{\epsilon} f_{\mu}^{(0)} \delta\epsilon_{\mu}) O_{\mu}(\mathbf{k})$. Noting that $\partial_{\epsilon} f_{\mu}^{(0)}(\mathbf{k}) = -\delta(\epsilon_{\mu}(\mathbf{k}) - E_f)$ at zero temperature, i.e., the integrand in Eq. (26) only has a finite value on the Fermi surface, it becomes evident that $\delta O^{(1)}$ is the change in O due to the first-order change in the occupancy of the states in the vicinity of the original Fermi surfaces caused by the electric-induced shifts of the Fermi surfaces. This is schematically illustrated for $O = v_x$ and an applied electric field along the x direction in Fig. 1 for a single band (the band index μ is omitted in the figure for simplicity). In the RTA, $\delta\epsilon_{\mu}$ is proportional to $\langle v_x \rangle$. In Fig. 1(a), the portions of $O(\mathbf{k})$ multiplied by positive (negative) values of $\delta f^{(1)}$ in

Eq. (26) corresponding to states with positive (negative) values of $\langle v_x \rangle$ are denoted in green (red). The states on the left half of the Fermi surface with negative velocities parallel to the electric field correspond to previously occupied states which now became unoccupied because their states got scattered into states with more positive values of k_x by the electric field. This loss in occupancy results in a reduction of the total energy of the occupied states on the left half of the Fermi surface and a negative $\delta\epsilon_\mu$ because there are now fewer occupied states. Conversely, the previously unoccupied states with energies slightly higher than the Fermi energy on the right half of the Fermi surface that now become occupied, thereby corresponding to a gain in energy of the occupied states and a positive $\delta\epsilon_\mu$ because there are now more occupied states there.

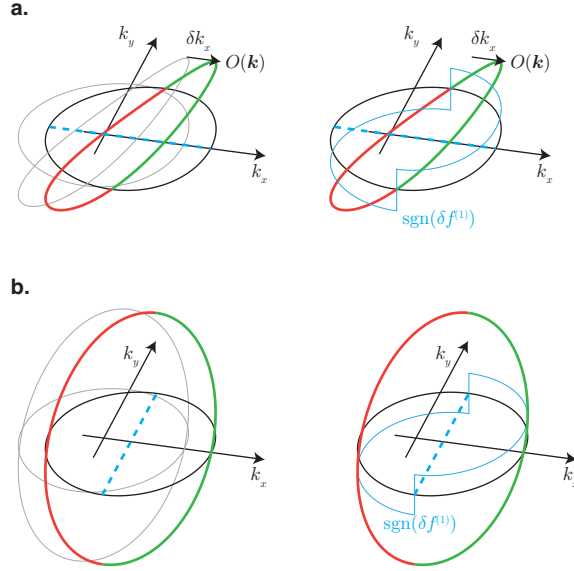


FIG. 1. A schematic illustration of the first-order change $\delta O^{(1)}$ for (a) the observable $O = v_x$ in a system coupled to a magnetization in the y direction, for which the Fermi surface is symmetrical about the k_x axis, and (b) the observable $O = v_y$ in a system coupled to a magnetization in the x direction, for which the Fermi surface is symmetrical about the k_y axis. The symmetry axes of the systems are denoted by the blue dotted lines along the k_x or k_y axes. The lighter gray ellipsoids on the $k_x - k_y$ plane in the left plots represent the original Fermi surfaces, the black ellipsoids are the Fermi surfaces shifted by δk_x due to an applied electric field in the x direction, and the lighter gray curves the values of $O(\mathbf{k})$ on the original Fermi surface. The blue half-ellipsoids denoted as $\text{sgn}(\delta f^{(1)})$ in the right plots denote the sign of the first-order change in the Fermi-Dirac occupancy factor where the portions above (below) the $k_x - k_y$ plane denote a positive (negative) value. The portions of $O(\mathbf{k})$ in green (red) are multiplied by positive (negative) values of $\delta f^{(1)}$ in the expressions for $\delta O^{(1)}$.

The second order change in O , $\delta O^{(2)}$, has the following interpretation. Analogous to Eq. (26), $\delta O^{(2)}$ is given by

$$\delta O^{(2)} = \sum_{\mu} \int d\mathbf{k} \left(\delta f_{\mu}^{(2)}(\mathbf{k}) O_{\mu}(\mathbf{k}) \right). \quad (27)$$

Substituting Eq. (25) into Eq. (24) gives

$$\delta O^{(2)} = - \sum_{\mu} \int d\mathbf{k} \left((\partial_{\epsilon} \delta f_{\mu}^{(1)}) (\delta \epsilon_{\mu} O_{\mu}) \right) \quad (28)$$

$$= - \sum_{\mu} \int d\mathbf{k} \left[\partial_{\epsilon} (\delta \epsilon_{\mu} \delta f_{\mu}^{(1)} O_{\mu}) - \partial_{\epsilon} (\delta \epsilon_{\mu} O_{\mu}) (\delta f_{\mu}^{(1)}) \right] \quad (29)$$

$$= \sum_{\mu} \int d\mathbf{k} \left[(\partial_{\epsilon} \delta \epsilon_{\mu}) O_{\mu} + \delta \epsilon_{\mu} (\partial_{\epsilon} O_{\mu}) \right] (\delta f_{\mu}^{(1)}). \quad (30)$$

In going from Eq. (29) to Eq. (30), we made use of the fact that the integration limits of \mathbf{k} span from $\epsilon_{\mu} = -\infty$ to ∞ while the $\partial_{\epsilon} (\delta \epsilon_{\mu} \delta f_{\mu}^{(1)} O_{\mu})$ term in the integration contains a factor of $\delta(\epsilon - \epsilon_{\text{F}})$ within $\delta f_{\mu}^{(1)}$. This term therefore does not contribute to the integral because the delta function is zero at the integration limits of ϵ_{μ} and can be omitted.

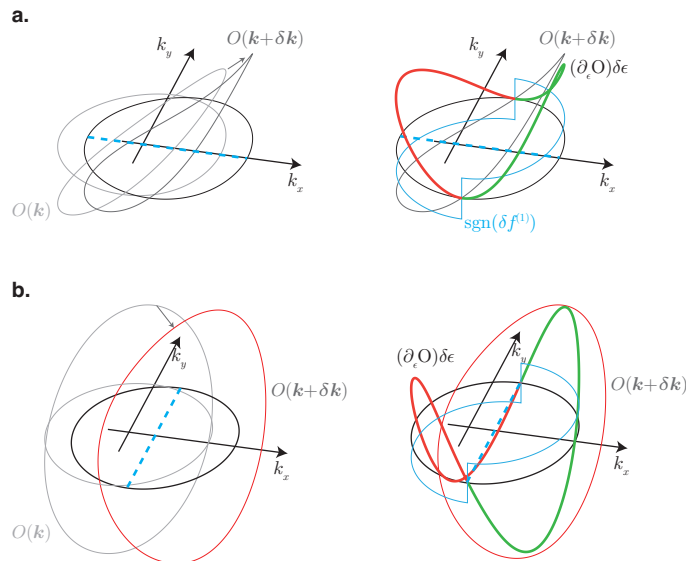


FIG. 2. A schematic illustration of the $(\partial_\epsilon O)\delta\epsilon$ second-order changes in a single band for (a) the observable $O = v_x$ in a system coupled to a magnetization in the y direction, for which the Fermi surface is symmetrical about the k_x axis, and (b) the observable $O = v_y$ in a system coupled to a magnetization in the x direction, for which the Fermi surface is symmetrical about the k_y axis. The symmetry axes of the systems are denoted by the blue dotted lines along the k_x or k_y axes. The lighter gray ellipsoids in the left plot on the $k_x - k_y$ plane represent the original Fermi surfaces and the lighter gray curves the values of $O(\mathbf{k})$ on the original Fermi surface. The black ellipsoids and the darker gray lines in the left and right plots represent the shifted Fermi surfaces and the values of $O(\mathbf{k} + \delta\mathbf{k})$ on the shifted Fermi surfaces, respectively. The blue half-ellipsoids denoted as $\text{sgn}(\delta f^{(1)})$ on the right plots denote the sign of the first-order change in the Fermi-Dirac occupancy factor where the portions above (below) the $k_x - k_y$ plane denote a positive (negative) value. The portions of $(\partial_\epsilon O)\delta\epsilon$ in the right plots in green (red) are multiplied by positive (negative) values of $\delta f^{(1)}$ in the expressions for $\delta O^{(1)}$ and $\delta O^{(2)}$.

The integrand in Eq. (30) contains two terms. The first term $(\partial_\epsilon \delta\epsilon_\mu)\delta f_\mu^{(1)}O_\mu$ accounts for the energy dependence of $\delta\epsilon$ itself (both $\mathbf{v}(\mathbf{k})$ in $\delta\epsilon$ and the eigenenergy $\epsilon(\mathbf{k})$ are functionally related through their common dependence on \mathbf{k}). Substituting Eq. (13) for $\delta f_\mu^{(1)}$ into the expression gives

$$(\partial_\epsilon \delta\epsilon_\mu)\delta f_\mu^{(1)} = -(\partial_\epsilon f_\mu^{(0)})[(\partial_\epsilon \delta\epsilon_\mu)\delta\epsilon_\mu]. \quad (31)$$

The term in the square brackets on the right hand side can be interpreted as a change in energy that is second order in E , $\delta\epsilon_\mu^{(2)} \equiv (\partial_\epsilon \delta\epsilon_\mu)\delta\epsilon_\mu$ so that the term in Eq. (31) can be written as $\delta\epsilon_\mu^{(2)}\partial_\epsilon f_\mu^{(0)}$. This has the physical interpretation of a change in the Fermi-Dirac distribution occupancy factor arising from the second-order shift in energy due to the displacement of the Fermi surface. The second term in the integrand in Eq. (30), $(\partial_\epsilon O_\mu\delta\epsilon_\mu)(\delta f_\mu^{(1)})$ is a product of two factors. The first term $(\partial_\epsilon O_\mu\delta\epsilon_\mu)$ corresponds to the change in the expectation value of O at \mathbf{k} on the Fermi surface of the μ th band due to the Fermi surface shift from \mathbf{k} to $\mathbf{k} + \delta\mathbf{k}$ (Fig. 2). The second term $\delta f_\mu^{(1)}$ corresponds to the first-order change in the occupancy factor of the states in the vicinity of the original Fermi surface due to the k -space shift of the Fermi surface.

III. SYMMETRY ANALYSIS

We apply the general results obtained in the previous section to the specific case of the low-energy Hamiltonian for the lowest-energy pair of spin states in the LaO/STO system. Including the cubic spin-orbit coupling terms, the Hamiltonian is given by [19]

$$H = \frac{k^2}{2m^*} + J_H \boldsymbol{\sigma} \cdot \mathbf{M} + \alpha(\boldsymbol{\sigma} \times \mathbf{k}) \cdot \hat{z} + \sigma_x \beta_3 (k_y k_x^2 - k_y^3) - \sigma_x \eta_3 k_x^2 k_y + \sigma_y \beta_3 (k_x k_y^2 - k_x^3) + \sigma_y \eta_3 k_y^2 k_x \quad (32)$$

where α represents the strength of the linear Rashba SOC (RSOC), β_3 and η_3 are coefficients of the two distinct cubic SOC terms, and J_H the Heisenberg exchange interaction between conduction electrons and the magnetic moments of the dopants \mathbf{M} . The effects of each of these RSOI terms on the Fermi surfaces and spin polarizations have been

O	Sym. O	Sym $\delta O^{(1)}$	Sym $\delta O^{(2)}$
v_x	+	+	+
v_y	-	-	-
σ_x	-	-	-
σ_y	+	+	+
j_{xy}	+	+	+
j_{yy}	-	-	-

TABLE I. Symmetries of various observables and their first- and second-order responses w.r.t. the k_x symmetry axis for magnetization \mathbf{M} and electric field aligned along the y and x axes, respectively. + and - denote symmetric and anti-symmetric, respectively.

described in more detail previously [25]. Here, we consider the effects of coupling to magnetic dopants that have moments lying in the in-plane direction $\mathbf{M} = M(\cos(\phi_m)\hat{x} + \sin(\phi_m)\hat{y}) = M_x\hat{x} + M_y\hat{y}$.

As before, we assume that the electric field is applied along the x direction. To understand which observables have finite first- and second-order response, we consider the symmetry properties of the LaO-STO system when the moment magnetization is aligned along the x or y directions.

When \mathbf{M} is aligned along the y direction, the Hamiltonian Eq. (32) becomes invariant under the transformation $(k_x, k_y, \sigma_x, \sigma_y) \rightarrow (k_x, -k_y, -\sigma_x, \sigma_y)$. These symmetry properties imply that $\langle \sigma_x \rangle$ is antisymmetric and $\langle \sigma_y \rangle$ symmetric about the k_x axis. At the same time, $\langle v_x \rangle$ is symmetric and $\langle v_y \rangle$ antisymmetric about the same k_x axis. As for the spin current $j_{i\alpha}$ where i and α respectively denote the current flow and spin directions, the overall symmetry is given by the product of the individual symmetries of $\langle v_i \rangle$ and $\langle \sigma_\alpha \rangle$. Hence, $\langle j_{yy} \rangle$ is antisymmetric and $\langle j_{xy} \rangle$ is symmetric with respect to the k_x axis.

Let us consider the k -space symmetry of the first-order response. From Eq. (26), the first-order response is the k -space integral of the product of O_μ and $\delta f_\mu^{(1)}$. By considering Eq. (24) and noting that in RTA, $\delta\epsilon_\mu = eE\langle v_x \rangle\tau$, $\delta f_\mu^{(1)}$ has the same symmetry as $\langle v_x \rangle$, i.e., it is symmetric about the k_x axis. Therefore, the symmetry of the integrand about the k_x axis in Eq. (26) is given by the product of the symmetry of O and the even symmetry of $\langle v_x \rangle$. Hence, for an O_μ that is antisymmetric about the k_x axis, the integral cancels out to zero after the k -space integration over the entire Fermi surface. Note that the converse result does not necessarily hold, i.e., an observable O_μ that is symmetric about the k_x axis will not necessarily result in a finite response (e.g. it may still integrate to zero if the k_y axis is an antisymmetry axis.) For the example of $O = v_x$ shown in Fig. 1a, the finite M_y breaks the exact symmetry about the k_y axis by causing an elongation of the Fermi surface along the k_x axis (as can be seen from the sharper curvature of the Fermi surface at negative values of k_x), thus resulting in a finite first-order response.

The symmetry properties of the second-order response are determined by those of its two constituent components given in Eq. (30). The product $(\partial_\epsilon\delta\epsilon_\mu)(\delta f_\mu^{(1)})$ in the first term is symmetric about the k_x axis because both $\partial_\epsilon\delta\epsilon_\mu$ and $\delta f_\mu^{(1)}$ have the same symmetries about the k_x axis. The symmetry of the former can be seen from the following argument: Consider the expectation value of a generic observable O at point (k_x, k_y) on the Fermi surface of the μ th band $O_\mu(k_x, k_y)$ where $O_\mu(k_x, k_y) = \pm O_\mu(k_x, -k_y) \forall k_x, k_y$. By definition, for a given energy ϵ and k_x ,

$$\partial_\epsilon O_\mu(k_x, k_y) = \lim_{\delta\epsilon \rightarrow 0} [O_\mu(k_x, k_y(\epsilon + \delta\epsilon, k_x)) - O_\mu(k_x, k_y(\epsilon, k_x))]/\delta\epsilon \quad (33)$$

$$= \pm \lim_{\delta\epsilon \rightarrow 0} [O_\mu(k_x, -k_y(\epsilon_F + \delta\epsilon, k_x)) - O_\mu(k_x, -k_y(\epsilon_F, k_x))]/\delta\epsilon \quad (34)$$

$$= \pm \partial_\epsilon O_\mu(k_x, -k_y) \quad (35)$$

where we have explicitly written k_y on the Fermi surface as a function of the ϵ_F and k_x . Equations (33)–(35) show that $\partial_\epsilon O_\mu$ has the same symmetry as O_μ about a symmetry axis. Since $\delta f_\mu^{(1)}$ is proportional to $\delta\epsilon_\mu$, both $(\partial_\epsilon\delta\epsilon_\mu)$ and $\delta f_\mu^{(1)}$ have the same symmetries about the k_x axis. Their product is therefore symmetric. The symmetry of $(\partial_\epsilon\delta\epsilon_\mu)(\delta f_\mu^{(1)})O_\mu$ about the k_x axis is thus determined by that of O_μ . We now consider the second component in Eq. (30), i.e., $(\partial_\epsilon O_\mu\delta\epsilon_\mu)(\delta f_\mu^{(1)})$. As explained, the symmetry of $\partial_\epsilon O_\mu$ about the k_x symmetry axis is the same as that of O_μ itself, while the product of the remaining $(\delta\epsilon_\mu)(\delta f_\mu^{(1)})$ terms is symmetric (Fig. 2a) since $\delta f_\mu^{(1)}$ is proportional to $\delta\epsilon_\mu$. Therefore, putting everything together, the symmetry of the integrand in Eq. (30) about the k_x axis when the electric field is along the x direction and in the presence of a finite M_y will be the same as that of O_μ . The second-order responses for v_y and σ_x are therefore antisymmetric about the k_x axis and cancel out to zero. The symmetry properties of the various observables and their first- and second-order responses are summarized in Table I.

O	Sym. O	Sym. $\delta O^{(1)}$	Sym. $\delta O^{(2)}$
v_x	-	+	-
v_y	+	-	+
σ_x	+	-	+
σ_y	-	+	-
j_{xx}	-	+	-
j_{yx}	+	-	+

TABLE II. Symmetries of various observables and their first- and second-order responses w.r.t the k_y symmetry axis for magnetization \mathbf{M} and electric field both along the x axis. + and - denote symmetric and anti-symmetric, respectively.

We now consider the case where \mathbf{M} is aligned along the x direction. The Hamiltonian Eq. (32) is now invariant under the transformation $(k_x, k_y, \sigma_x, \sigma_y) \rightarrow (-k_x, k_y, \sigma_x, -\sigma_y)$ and the k_y axis is a symmetry axis of the system (Fig. 2b). Thus, $\langle v_y \rangle$, $\langle \sigma_x \rangle$, and $\langle j_{yx} \rangle$ are symmetric about the k_y axis, while $\langle v_x \rangle$, $\langle \sigma_y \rangle$, and $\langle j_{xx} \rangle$ are antisymmetric. In marked contrast to the M_y -magnetized system discussed earlier where $\langle v_x \rangle$ is symmetric about its symmetry axis along the k_x axis, in the M_x -magnetized system, $\langle v_x \rangle$ and therefore $\delta\epsilon$, are antisymmetric about the symmetry axis along the k_y axis. Therefore, the first-order responses for O_μ will have the opposite symmetries w.r.t. the k_y axis compared to that of the parent O_μ . However, the arguments presented in the previous paragraph for the symmetry of the second-order response of O_μ are still applicable here. Because both $(\partial_\epsilon \delta\epsilon_\mu)$ and $\delta f^{(1)}$ are *anti*-symmetric about the k_y symmetry axis, their product and therefore the second-order response would still be symmetric about that axis. Thus, the second-order response shares the same symmetry about the k_y axis as O_μ (Fig. 2b). The symmetry properties of various observables and their first- and second-order responses are summarized in Table II.

Comparing the results in Tables I and II, it can be seen that for the observables listed, the first- and second-order responses have the same (opposite) symmetries with respect to the symmetry axis of k_x when \mathbf{M} is along the y (x) direction. This implies that in the M_x -magnetized system, a finite first-order response for an observable is accompanied by a finite second-order response, whereas in the M_y -magnetized system, we can have the remarkable situation of a finite second-order response for an observable without a net first-order response. For illustration, we present exemplary numerical calculations in the next section.

IV. RESULTS AND DISCUSSION

For all the numerical results that follow, we take $J_H M = 10$ meV and $\epsilon_F = 30$ meV from the band bottom of the le^- band, at which Eq. (32) is a good description of the electronic behavior of the LaO-STO system [25]. The SOC strengths α , β_3 , and η_3 in Eq. (32) are treated as free parameters and varied over a range of -10 to 10 meVÅ for α and from -3 to 3 eVÅ³ for β_3 and η_3 , based on the values in Ref. [19] for typical thicknesses and out-of-plane electric fields in LaO/STO quantum well structures. In keeping with the commonly used symbols for the various quantities, we define the charge currents $\delta J_{x,y}^{(1,2)}$, spin accumulations $\delta S_{x,y}^{(1,2)}$, and spin currents $\delta J_{x,y;x,y}^{(1,2)}$, as $\delta O^{(1,2)}$ in Eqs. (26) and (30) with $O = v_{x,y}$, $\sigma_{x,y}$, and $\frac{1}{2}\{v_{x,y}, \sigma_{x,y}\}$, respectively. All the results that follow were obtained using the SL approach.

Fig. 3 shows the first- and second-order responses for the charge current parallel ($\delta J_x^{(1,2)}$) and perpendicular ($\delta J_y^{(1,2)}$) to the applied electric field as functions of the magnetization angle (ϕ_m) and SOC strength β_3 . In agreement with the predictions in Table II based on symmetry arguments, $\delta J_x^{(1)}$ and $\delta J_x^{(2)}$ have finite values while $\delta J_y^{(1)}$ and $\delta J_y^{(2)}$ integrate to zero when $\phi_m = 0, \pi$, which correspond to \mathbf{M} lying along the $\pm x$ directions. Similarly, the finite values for $\delta J_x^{(1)}$ and $\delta J_y^{(2)}$ and zero net values for $\delta J_y^{(1)}$ and $\delta J_x^{(2)}$ at $\phi_m = \pm\pi/2$, corresponding to \mathbf{M} along the $\pm y$ directions, are consistent with the the predictions in Table I. Similarly, we also evaluated the spin accumulations perpendicular to the magnetization ($\delta S_\perp^{(1/2)}$) and spin currents with spin parallel to the magnetization and flowing parallel and perpendicular to the electric field $\delta J_{(x,y)\parallel}^{(1/2)}$ as functions of ϕ_m and β_3 . The corresponding first- and second-order responses are all in agreement with Tables I and II, as shown in the plots in Supplementary Materials Fig. S2.

At intermediate magnetization angles between the $\pm x, y$ directions, the symmetries / antisymmetries described in Sect. III do not hold exactly. As a result, the magnitudes of the first- / second- order responses that are exactly symmetric about their respective symmetry axes when the magnetization angles are along the $\pm x$ or $\pm y$ direction would now decrease as we move away from the symmetry axes owing to partial cancellation by the emergent antisymmetric contributions at the intermediate angles. Conversely, the first- / second-order responses that are exactly antisymmetric about their respective symmetry axes would now acquire a finite net value at the intermediate

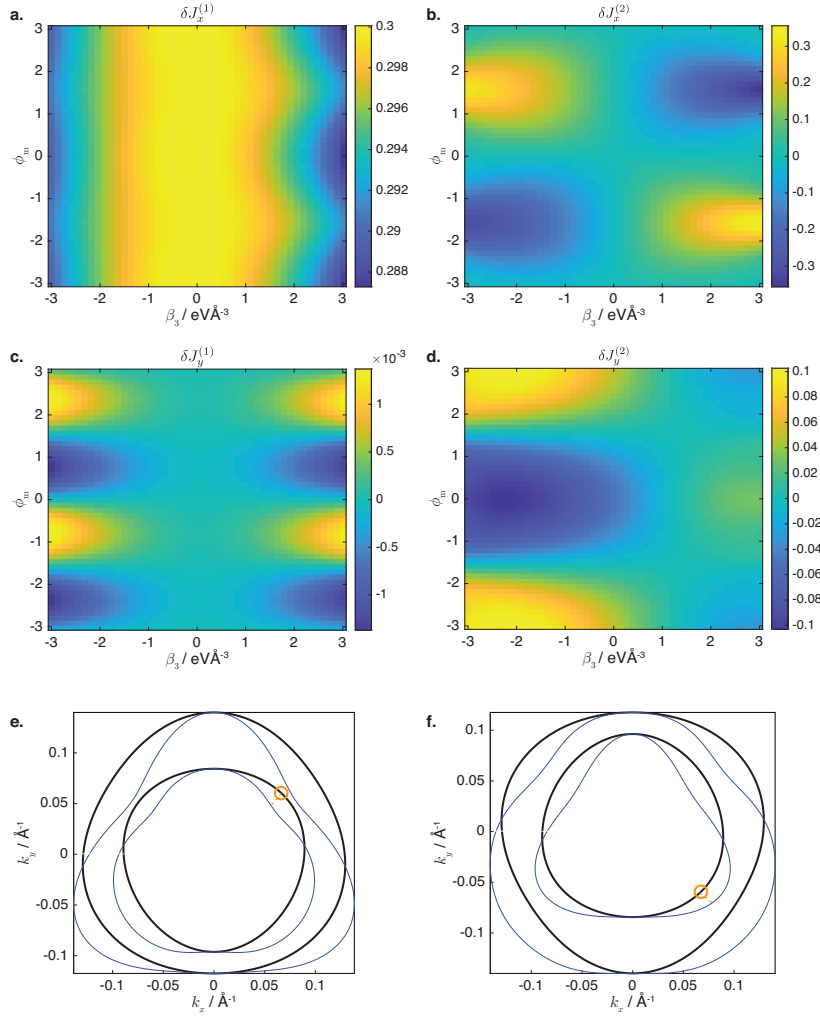


FIG. 3. (a) First- ($\delta J_x^{(1)}$) and (b) second-order responses ($\delta J_x^{(2)}$) for current parallel to applied electric field, and (c) first- ($\delta J_y^{(1)}$) and (d) second- ($\delta J_y^{(2)}$) order responses in $e = \hbar = 1$, eV, \AA units and unit electric field for current perpendicular to electric field as functions of the magnetization direction ϕ_m and the β_3 SOC parameter for $\alpha = 5 \text{ meV}\text{\AA}$ and $\eta_3 = 1 \text{ meV}\text{\AA}^3$. (e) and (f) show the Fermi surfaces (thick black curves) and the sign and magnitude of the contribution of each state on the Fermi surfaces (thin blue lines) to $\delta J_x^{(2)}$ for magnetizations along the (e) $-x$ and (f) $+x$ directions at $\beta_3 = 3 \text{ meV}\text{\AA}^3$. (The sign of the contribution of each state on the Fermi surface to $\delta J_x^{(2)}$ is indicated by whether its corresponding point on the blue curve lies within (negative value) or outside the Fermi surface (positive value), and its relative magnitude by the separation between that point and the Fermi surface. The circles in (e) and (f) indicate a pair of states with opposite signs of the x magnetization, k_y , and second-order contribution.

magnetization orientations due to imperfect cancellation. This gives rise to the approximately $\sin(\phi_m)$ variation of $\delta J_x^{(2)}$ in Fig. 3b, which is consistent with experimental results observed in the LaO/STO system[8], as well as the finite values of $\delta J_y^{(1)}$ in Fig. 3c and $\delta S_{\perp}^{(2)}$ in Fig. S2b at intermediate values of ϕ_m , whereas both quantities go to zero at $\phi_m = 0, \pm\pi/2$ due to perfect cancellation.

An interesting point to note is that the signs of the second-order responses for the charge current in the $i = (x, y)$ direction flips when the magnetization direction is reversed about the i axis, as shown in Fig. 3b and d. The origin of this flip was alluded to in the discussion on Fig. 2a, where we noted that for a finite response to be obtained for \mathbf{M} along the y -direction, not only should the quantity be symmetric about its k_x symmetry axis, but additionally its antisymmetry about the k_y axis should also be broken. This antisymmetry is broken by the applied magnetization. We show the breaking of the antisymmetry by the magnetization more explicitly in Fig. 3e and f, which show the Fermi surfaces and second-order contributions to $J_y^{(2)}$ for magnetizations applied along the $-x$ and $+x$ directions, respectively. The Fermi surfaces for the two magnetization directions are reflections of each other about the k_x axis.

This can be shown analytically by considering the eigenvalues of Eq. (32), which are given by

$$\epsilon_\mu = \frac{k^2}{2m^*} \pm \sqrt{(J_H M_x + k_y(\alpha - k_y^2 \beta_3 + k_x^2(\beta_3 - \eta_3)))^2 + (J_H M_y - k_x(\alpha + k_x^2 \beta_3 - k_y^2(\beta_3 - \eta_3)))^2}, \quad (36)$$

and is invariant under $(M_x, k_y) \rightarrow (-M_x, -k_y)$ when $M_y = 0$. For simplicity, we denote the eigenvalue as ϵ_μ^\pm when $M_y = 0$ and $M_x = \pm|M_x|$. Thus, we have $\epsilon_\mu^-(k_x, k_y) = \epsilon_\mu^+(k_x, -k_y)$. By definition, $\langle v_y^\pm(k_x, k_y) \rangle = \partial_{k'_y} \epsilon_\mu^\pm(k_x, k'_y)$. Setting $k'_y = \pm k_y$ yields $\langle v_y^\pm(k_x, k_y) \rangle = \pm \langle v_y^\pm(k_x, \pm k_y) \rangle$. (More intuitively, this can be seen by noting that for states that are particle-like, the Fermi surfaces become larger with increasing energy so the states with large positive (negative) values of k_y extend upwards with increasing energy and have positive (negative) expectation values for v_y regardless of whether the magnetization is along the $+x$ or $-x$ directions.) Therefore, the contribution to the second-order response, $\delta J_y^{(2)}$, of a state at (k_x, k_y) on the Fermi surface in the $+x$ magnetized system has the same magnitude but opposite sign to that of the corresponding state at $(k_x, -k_y)$ in the $-x$ magnetized system (compare Fig. 3e and f). The net resultant value of $\delta J_y^{(2)}$ therefore has the same magnitude but opposite signs when the magnetization direction switches from $+x$ to $-x$ after integrating over the entire Fermi surface and summing up over both bands. (Although the argument provided pertains to only the $\pm x$ magnetization directions, it can be generalized to magnetization directions along any arbitrary axis.)

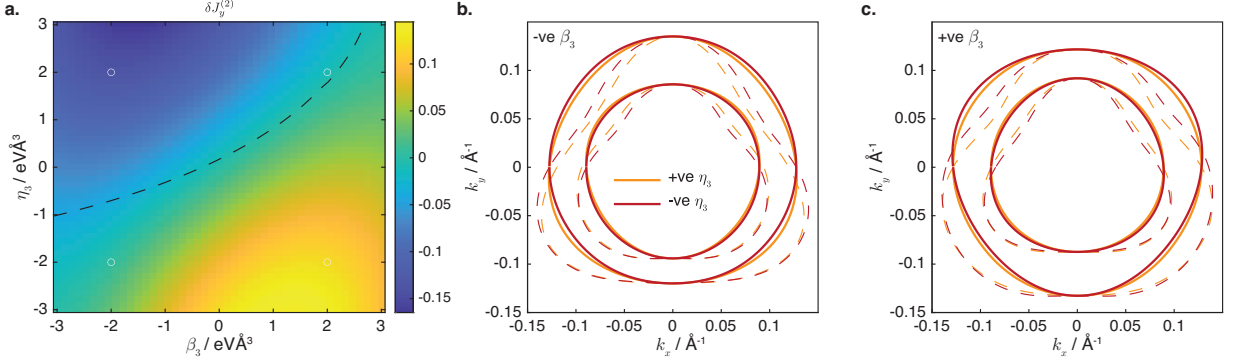


FIG. 4. (a) Variation of $\delta J_y^{(2)}$ with η_3 and β_3 at $\alpha = 5$ meV \AA and $\phi_m = 0$. The dotted line traces the loci of η_3 and β_3 at which $\delta J_y^{(2)} = 0$. (b) and (c) show the Fermi surfaces and the sign and magnitudes of the relative contributions for each state on the Fermi surfaces for $\eta_3 = \pm 2$ meV \AA and (b) $\beta_3 = -2$ meV \AA^3 and (c) $\beta_3 = 2$ meV \AA^3 . The sign of the contribution of each state on the Fermi surface to $\delta J_y^{(2)}$ is indicated by whether its corresponding point on the dotted line of the same color lies within (negative value) or outside the Fermi surface (positive value), and its relative magnitude by the separation between that point and the Fermi surface. The points $\eta_3 = \pm 2$ meV \AA^3 and $\beta_3 = \pm 2$ meV \AA^3 depicted in panels (b) and (c) are marked by the white circles in (a).

We next consider the effect of the cubic SOC terms on the second-order Hall charge current response when the magnetization is parallel to the electric field. (The first-order charge current is zero, as shown in Table I.) Fig. 4a shows that the sign and magnitude of $\delta J_y^{(2)}$ can be under varying η_3 and / or β_3 . As discussed earlier, the net value of $\delta J_y^{(2)}$ is given by the sum of contributions from the states integrated over the Fermi surfaces of the two bands, as shown in Fig. 4b and c. Because the contributions from each state does not all have the same sign, the sign of the net $\delta J_y^{(2)}$ after summing over all states depends on the balance between the positive and negative contributions on the Fermi surfaces. This in turn is determined by (i) the magnitude of the contribution of each state and (ii) the portions on the Fermi surfaces occupied by states with positive and negative contributions. For example, at $\beta_3 = -2$ meV \AA^3 , $\delta J_y^{(2)}$ is negative at $\eta_3 = 2$ meV \AA^3 and positive at $\eta_3 = -2$ meV \AA^3 as shown in Fig. 4a. The Fermi surfaces and contributions of each state to $\delta J_y^{(2)}$ corresponding to these values of β_3 and η_3 are shown in Fig. 4b. We focus on the outer Fermi surface, which has a larger k -space length corresponding to more states and therefore plays a larger role in determining the net value of $\delta J_y^{(2)}$. The negative value of $\delta J_y^{(2)}$ at $\eta_3 = 2$ meV \AA^3 can then be explained by the larger magnitude of the negative contributions from states at the top half of the Fermi surface (note that the dark yellow dotted line for $\eta_3 = 2$ meV \AA^3 cuts a deeper recess into the Fermi surface), as well as the larger portion of the Fermi surface occupied by states with negative contributions (the contributions switch to positive at a larger value of k_y compared to the corresponding case of $\eta_3 = -2$ meV \AA^3). Fig. 4c shows a complementary example for $\beta_3 = 2$ meV \AA^3 where the magnitude of the negative $\delta J_y^{(2)}$ is smaller than that at $\beta_3 = -2$ meV \AA^3 keeping the other cubic

SOC parameter fixed at $\eta_3 = 2 \text{ meV}\text{\AA}^3$. The decrease in the magnitude of $\delta J_y^{(2)}$ in the former can be attributed to the fact the portions of the outer Fermi surface with negative contributions now constitute a smaller proportion of the total length of the Fermi surface.

Lastly, the plot in Fig. 4a indicates that η_3 has a larger influence on the sign of $\delta J_y^{(2)}$ than β_3 . (This can be seen from the fact that the dotted line denoting the locus of $\delta J_y^{(2)}$ lies closer to the horizontal line, which indicates that the sign of $\delta J_y^{(2)}$ is independent of β_3 , than the vertical line, which indicates that the sign of $\delta J_y^{(2)}$ is independent of η_3 .) The larger influence of η_3 can also be seen by rewriting the energy eigenvalues in Eq. (36) in polar coordinates

$$\begin{aligned} \epsilon_\mu = & \frac{k^2}{2m^*} \pm \left((-k\alpha \sin(\phi) + k^3(\beta_3 + \eta_3) \cos^2(\phi) \sin(\phi) - k^3 \sin^3(\phi)) \right. \\ & \left. + (J_H M_x + k\alpha \cos(\phi) + k^3(\beta_3 - \eta_3) \cos(\phi) \sin^2(\phi) - k^3 \beta^3 \cos(\phi)^3) \right)^{\frac{1}{2}}, \end{aligned} \quad (37)$$

from which it can be seen that the terms containing η_3 have the largest magnitudes at $\phi = \pm\pi/4, \pm3\pi/4$. These values of ϕ coincide with those at which the contributions to $\delta J_y^{(2)}$ have the largest magnitudes. Note that the contributions to $\delta J_y^{(2)}$ go to zero at $\phi = \pm\pi/2$ since $\langle v_x \rangle = 0$, which leads to $\delta\epsilon_\mu = 0$ by Eq. (30), and also at $\phi = 0, \pi$ where $\langle v_y \rangle = 0$. Therefore, changing the value of η_3 would cause a relatively large change in the contribution to $\delta J_y^{(2)}$. At the same time, changing the sign of η_3 also has the significant effect of changing the shape of the Fermi surfaces and therefore, the relative lengths of the portions with positive and negative contributions to $\delta J_y^{(2)}$ (see Fig. 4b and c.) This is compatible with experimentally findings that reveal the sensitivity of the second-order response in WTe_2 to the shape of the Fermi surface [2].

V. CONCLUSIONS

In this study, we investigated the second-order spin accumulation and spin and charge current responses to an applied electric field in a LaO/STO system in the presence of cubic SOC terms and magnetic dopants. We first extended the approach of Schliemann and Loss for solving the Boltzmann transport equation to higher orders in the applied electric field. We then explained the physical origin of the second-order response of an observable quantity as the combined effects of the change in the expectation value due to the Fermi surface shift and the energy dependence of the shift. Subsequently, we performed a symmetry analysis on the LaO/STO system when the magnetization of the dopants lies parallel or perpendicular to the applied electric field. We showed how the interplay between the magnetization direction and the shift in the Fermi surface shift leads to antisymmetrical distributions of some of the observable quantities, which results in the cancellation of their corresponding first- or second-order responses in some cases. Conversely, in other cases broken antisymmetry results in finite responses. These theoretical predictions were subsequently confirmed by numerical calculations. Finally, we further explored the magnetization direction dependence of the first- and second-order responses and the interplay between the two cubic RSOC strength. We showed that the sign of the second-order responses can be switched by varying either the magnetization direction or relative magnitudes of the cubic RSOC terms, a finding that may be explained by the k -space symmetry of the Fermi surfaces of the system. These findings extend our understanding of how the spin and charge responses are affected by the interplay between multiple SOC effects in a LaO/STO system, and how the relative magnitudes of the first- and second-order responses of various quantities can be engineered for practical applications by exploiting the symmetries of the system.

ACKNOWLEDGMENTS

This work is supported by the Ministry of Education (MOE) Tier-II Grant No. MOE-T2EP50121-0014 (NUS Grant No. A-8000086-01-00), and MOE Tier-I FRC grant (NUS Grant No. A-8000195-01-00).

-
- [1] T Ideue, K Hamamoto, S Koshikawa, M Ezawa, S Shimizu, Y Kaneko, Y Tokura, N Nagaosa, and Y Iwasa. *Nat. Phys.*, 13(6):578–583, 2017.
- [2] Pan He, Chuang-Han Hsu, Shuyuan Shi, Kaiming Cai, Junyong Wang, Qisheng Wang, Goki Eda, Hsin Lin, Vitor M Pereira, and Hyunsoo Yang. Nonlinear magnetotransport shaped by fermi surface topology and convexity. *Nat. Commun.*, 10:1290, 2019.

- [3] Pan He, Steven S-L Zhang, Dapeng Zhu, Yang Liu, Yi Wang, Jiawei Yu, Giovanni Vignale, and Hyunsoo Yang. Bilinear magnetoelectric resistance as a probe of three-dimensional spin texture in topological surface states. *Nat. Phys.*, 14(5):495–499, 2018.
- [4] Pan He, S McKeown Walker, Steven S-L Zhang, Flavio Yair Bruno, MS Bahramy, Jong Min Lee, Rajagopalan Ramaswamy, Kaiming Cai, Olle Heinonen, Giovanni Vignale, et al. Observation of out-of-plane spin texture in a sratio 3 (111) two-dimensional electron gas. *Phys. Rev. Lett.*, 120(26):266802, 2018.
- [5] Kaifei Kang, Tingxin Li, Egon Sohn, Jie Shan, and Kin Fai Mak. Nonlinear anomalous hall effect in few-layer wte2. *Nat. Mater.*, 18(4):324–328, 2019.
- [6] Hongyi Yu, Yue Wu, Gui-Bin Liu, Xiaodong Xu, and Wang Yao. Nonlinear valley and spin currents from fermi pocket anisotropy in 2d crystals. *Phys. Rev. Lett.*, 113(15):156603, 2014.
- [7] Pan He, Steven S-L Zhang, Dapeng Zhu, Shuyuan Shi, Olle G Heinonen, Giovanni Vignale, and Hyunsoo Yang. Nonlinear planar hall effect. *Phys. Rev. Lett.*, 123(1):016801, 2019.
- [8] Daeseong Choe, Mi-Jin Jin, Shin-Ik Kim, Hyung-Jin Choi, Junhyeon Jo, Inseon Oh, Jungmin Park, Hosub Jin, Hyun Cheol Koo, Byoung-Chul Min, et al. Gate-tunable giant nonreciprocal charge transport in noncentrosymmetric oxide interfaces. *Nat. Commun.*, 10(1):4510, 2019.
- [9] Diogo Castro Vaz, F Trier, A Dyrdał, Annika Johansson, Karin Garcia, Agnès Barthelemy, Ingrid Mertig, J Barnaś, Albert Fert, and M Bibes. Determining the rashba parameter from the bilinear magnetoresistance response in a two-dimensional electron gas. *Phys. Rev. Mater.*, 4(7):071001, 2020.
- [10] Jine Zhang, Hui Zhang, Xiaobing Chen, Jing Zhang, Shaojin Qi, Furong Han, Yuansha Chen, Weisheng Zhao, Fengxia Hu, Baogen Shen, et al. Anisotropic bilinear magnetoresistance in (110) sratio₃-based two-dimensional electron gas. *Phys. Rev. B*, 104(4):045114, 2021.
- [11] Yi Wang, Rajagopalan Ramaswamy, Mallikarjuna Motapothula, Kulothungasagaran Narayanapillai, Dapeng Zhu, Jiawei Yu, Thirumalai Venkatesan, and Hyunsoo Yang. Room-temperature giant charge-to-spin conversion at the sratio₃-laalo₃ oxide interface. *Nano Letters*, 17(12):7659–7664, Dec 2017.
- [12] Felix Trier, Diogo C. Vaz, Pierre Bruneel, Paul Noël, Albert Fert, Laurent Vila, Jean-Philippe Attané, Agnès Barthélémy, Marc Gabay, Henri Jaffrès, and Manuel Bibes. Electric-field control of spin current generation and detection in ferromagnet-free sratio₃-based nanodevices. *Nano Letters*, 20(1):395–401, Jan 2020.
- [13] J. Y. Chauleau, M. Boselli, S. Gariglio, R. Weil, G. de Loubens, J. M Triscone, and M. Viret. Efficient spin-to-charge conversion in the 2d electron liquid at the lao/sto interface. *EPL*, 116(1), OCT 2016.
- [14] K. V. Shanavas. Theoretical study of the cubic rashba effect at the sratio₃(001) surfaces. *Phys. Rev. B*, 93:045108, Jan 2016.
- [15] Haixing Liang, Long Cheng, Laiming Wei, Zhenlin Luo, Guolin Yu, Changgan Zeng, and Zhenyu Zhang. Nonmonotonically tunable rashba spin-orbit coupling by multiple-band filling control in sratio₃-based interfacial *d*-electron gases. *Phys. Rev. B*, 92:075309, Aug 2015.
- [16] H. Nakamura, T. Koga, and T. Kimura. Experimental evidence of cubic rashba effect in an inversion-symmetric oxide. *Phys. Rev. Lett.*, 108:206601, May 2012.
- [17] A. D. Caviglia, M. Gabay, S. Gariglio, N. Reyren, C. Cancellieri, and J.-M. Triscone. Tunable rashba spin-orbit interaction at oxide interfaces. *Phys. Rev. Lett.*, 104:126803, Mar 2010.
- [18] A. Fête, S. Gariglio, A. D. Caviglia, J.-M. Triscone, and M. Gabay. Rashba induced magnetoconductance oscillations in the laalo₃-sratio₃ heterostructure. *Phys. Rev. B*, 86:201105, Nov 2012.
- [19] Cong Son Ho, Weilong Kong, Ming Yang, Andrivo Rusydi, and Mansoor B A Jalil. Tunable spin and orbital polarization in SrTiO₃-based heterostructures. *New Journal of Physics*, 21(10):103016, oct 2019.
- [20] Zhuo Bin Siu, Mansoor BA Jalil, and Seng Ghee Tan. Effective hamiltonian for surface states of bi2te3 nanocylinders with hexagonal warping. *J. Phys. D: Appl. Phys.*, 49(22):225304, 2016.
- [21] Zhuo Bin Siu, Seng Ghee Tan, and Mansoor Jalil. Effective hamiltonian for surface states of topological insulator thin films with hexagonal warping. *AIP Advances*, 6(5):055706, 2016.
- [22] ZB Siu, MBA Jalil, and SG Tan. Topological state transport in topological insulators under the influence of hexagonal warping and exchange coupling to in-plane magnetizations. *Scientific Reports*, 4(1):5062, 2014.
- [23] John Schliemann and Daniel Loss. Anisotropic transport in a two-dimensional electron gas in the presence of spin-orbit coupling. *Phys. Rev. B*, 68:165311, Oct 2003.
- [24] Neil W. Ashcroft and N. David Mermin. *Solid State Physics*. Cengage Learning, 1976.
- [25] Anirban Kundu, Zhuo Bin Siu, and Mansoor BA Jalil. Semiclassical spin transport in lao/sto system in the presence of multiple rashba spin-orbit couplings. *New Journal of Physics*, 24(12):123045, 2023.

